Journal of Alloys and Compounds 909 (2022) 164634

Contents lists available at ScienceDirect

Journal of Alloys and Compounds

journal homepage: www.elsevier.com/locate/jalcom

Hydrothermal single crystal growth and structural investigation of the stuffed tridymite family as NLO materials

Rylan J. Terry[a,b], Daniel Vinton[a,b], Colin D. McMillen[a], Xiangfeng Chen[c,b], Lin Zhu[c,b], Joseph W. Kolis[a,b,*]

[a] Department of Chemistry, Clemson University, Clemson, SC 29634, USA
[b] Center for Optical Materials Science and Engineering Technologies (COMSET), Clemson University, Clemson, SC 29634, USA
[c] Department of Electrical and Computer, Clemson University, Clemson, SC 29634, USA

ARTICLE INFO

Article history:
Received 30 November 2021
Received in revised form 10 March 2022
Accepted 15 March 2022
Available online 19 March 2022

Keywords:
Hydrothermal synthesis
Nonlinear optics
Silicates
Germanates

ABSTRACT

The structures, crystal growth and preliminary NLO properties of a broad class of compounds known as the stuffed tridymites are investigated. The stuffed tridymites of the formula $ABCO_4$, where A are the alkali metal ions and *B* and *C* are Group 13 and 14 metal ions, respectively, form an extensive series of structures, all of which are based on symmetry breaking of the parent tridymite (SiO_2) structure. In all cases the alkali ion resides in channels running parallel to the *c*-axis formed from six-membered rings of tetrahedra of the metal ions. A large array of structures can be formed though combinations of ordering of the *B*/*C* sites, staggered and eclipsed tetrahedra, up/down orientations of the tetrahedra relative to the *c*-axis, and distortions of the six-membered rings. These symmetry breaking steps can be mixed and matched to form many different structures, and nearly all are in polar acentric space groups. The primary cause of centrosymmetric crystal formation is disorder of the *B*/*C* sites. When the sites are well ordered most of the structures are acentric with polar axes. High quality single crystals of most products can be grown using a high pressure hydrothermal method. Preliminary NLO experiments indicate that the compounds are acentric, but have low NLO conversions, which is expected due to the low polarizability of the building blocks. The extremely high percentage of polar acentric structure types, and the ability to correlate the structures to systematic variations of the very large and flexible tridymite structural class, suggests that this can serve as a starting point for designing crystals with many other useful physical properties.

1. Introduction

The absence of an inversion center in a crystal lattice provides an entry point to a wide range of interesting physical properties. One of the most important applications of acentric crystals is for nonlinear optics (NLO), but many other intriguing physical properties (e.g. frustrated magnetism, magnetooptics, multiferroics) all rely on some form acentricity in the crystal lattice. Fortunately, Neumann's rule enables the relatively straightforward sorting of physical properties by symmetry of the crystal groups [1–3]. It is well known that although the majority of space groups do not contain an inversion center, the percentage of actual crystal structures that adopt acentric space groups is extremely low (~15%), making the selection of materials for nonlinear optical applications very limited. Since there is not a reliable a priori method of predicting the adoption of acentric space groups, the design of acentric crystals is a unique challenge. Since the approach to obtaining new acentric materials is primarily an empirical one against unfavorable odds, we seek to look where the light is brightest and attempt to identify structural classes with relatively high tendencies to form acentric crystal types. We hope that this will provide valuable clues to the design of new acentric materials with interesting physical properties. In this regard we began to investigate a rich class of compounds known as stuffed tridymites [4–6].

The tridymites themselves are a class of structures within the quartz (SiO_2) family with an extensive and complex series of interrelationships based on the relative orientation of the silica tetrahedra, with symmetries ranging from the highest, $P6_3/mmc$, through multiple lower symmetry phases leading down to monoclinic symmetry. Such a range of structural variations is remarkable given that the only building blocks are corner sharing silica tetrahedra. Many of the structural variations can be accommodated using only subtle

* Correspondence to: 485H.L. Hunter Laboratories, Clemson, SC 29634, USA.
E-mail address: kjoseph@clemson.edu (J.W. Kolis).

https://doi.org/10.1016/j.jallcom.2022.164634
0925-8388/

perturbations of the rigid tetrahedra. One interesting fact is that nearly every lower symmetry variation of the parent hexagonal phase is in an acentric space group, making them attractive candidates for NLO and other acentric structure/property investigations.

The structural situation rapidly becomes even more complicated when it is realized that the channels running parallel to the dominant *c*-axis formed by the six membered rings can be occupied by a range of mono- or divalent cations that are normally alkali or alkaline earth cations, which can accommodate the variable coordination within the hexagonal columns. In that case the aliovalent substitutions within the so called stuffed tridymite series can lead to an enormous array of possible combinations with a general formula of $ABCO_4$. For example, the use of monovalent alkalis (*A*) as stuffing ions can lead to $ABSiO_4$ (*B* = Al^{3+}, Ga^{3+} etc.), while the use of divalent alkaline earths (*A*') can lead to *A*'*B*'SiO_4 (*B*' = Zn^{2+}, Co^{2+}, Ni^{2+} etc.). In addition, the silicate tetrahedra can be also replaced with other tetrahedra, such as in $ABPO_4$ [7–11], $ABAsO_4$ [12–14] or $RbMnVO_4$ [15]. In these various stuffed cases, all the building blocks, except for the stuffing ion, are tetrahedra. A critical aspect of the structural analysis is the ordering of the two different tetrahedral components. In most cases the sites order cleanly. This generally reduces the symmetry of the crystal, and the structural analysis can be treated as a coloring problem. In the relatively few cases where the sites disorder, the symmetry of the crystal is generally higher and centrosymmetric, and hence of less interest.

Even more than the pure unsubstituted tridymites (SiO_2), there is an astonishing array of structural possibilities for the $ABCO_4$ stuffed tridymite analogs, even when considering that again, all the *B* and *C* building blocks are tetrahedral. When the subtle variations of the tetrahedra couple with the coloring due to ordered *B* and *C* sites, a huge range of structural variations can be identified. What is particularly intriguing about the system is the exceptionally high percentage of different acentric space groups that form in this stoichiometric system. In fact, the overwhelmingly large number of structures form in noncentrosymmetric structures. This includes not just acentric but also polar and crystallographically chiral space groups [16]. This structural behavior is useful for physical properties beyond simple NLO behavior. It opens the door for many other important applications that require acentric structures, including spiral magnetic structures such as multiferroics, skyrmions, spintronics, magnetooptics, magnetoelectrics and many other next generation physical properties. The very high percentage of attractive space groups of the $ABCO_4$ tridymite derivatives makes this a very attractive hunting ground for interesting new materials.

In this work we investigate the chemistry, crystal growth and preliminary NLO properties of the stuffed tridymites where *A* is a monovalent alkali metal ion, *B* is a trivalent group 13 ion and *C* is a tetravalent group 14 ion. In all cases the *B* and *C* building blocks are tetrahedra. Using a high temperature hydrothermal synthetic procedure, we generally obtain high quality single crystals suitable for careful single crystal structural determination with good site ordering, and in many cases the crystals are large enough for NLO and other physical property measurements. There are a great many subtleties and ambiguities within even the "simplest" alkali aluminosilicates and their derivatives, so we found it necessary to start there to sort out some of the uncertainties in this structural class. Recently we reported on the deceptively complex structural chemistry of the Na^+ and K^+ aluminosilicate stuffed tridymites and found that they also form an unexpectedly high percentage of acentric space groups [17]. In this paper we systematically extend these investigations to the other elemental building blocks examining all the alkali ions and the heavier Group 13 and 14 ions. The Li^+ ions generally do not lead to tridymites but rather form acentric eucryptite derivatives ($LiAlSiO_4$ in *R*3) [18] which will be the subject of a subsequent report. A variety of structures as well as preliminary NLO data are reported. We view the designed growth of acentric crystals as only a first step to crystals displaying more complex physical properties. The identification of a chemically flexible class of compounds provides an excellent jumping off point to establish a test bed to obtain access to the broader class of tridymites that form in acentric, polar and chiral space groups. This may begin to afford a (slightly) designed approach to a wider range of single crystals capable of acting as multifunctional, emergent materials.

2. Experimental

2.1. Synthesis

Single crystals of the stuffed tridymite family having a basic formula of $ABCO_4$ were synthesized via hydrothermal reaction, where *A* is the stuffing cation (K, Rb, or Cs), *B* is the trivalent tetrahedral site (Al or Ga), and *C* is the tetravalent tetrahedral site (Si or Ge). $KGaSiO_4$, $RbAlSiO_4$, $CsAlSiO_4$ were synthesized using stoichiometric combinations of the basic oxides, however products containing germanium ($KAlGeO_4$ and $KGaGeO_4$, $RbAlGeO_4$, and $RbGaGeO_4$) required a 2:1 ratio with its trivalent component due to its high solubility under hydrothermal conditions. The synthesis of $CsGaSiO_4$ also necessitated a departure from the stoichiometric ratio to a 2:1 Ga:Si ratio in order to avoid the formation of $CsGaSi_2O_6$. To aid crystallization and act as the alkali nutrient source, 10 M *A*OH was used as a mineralizer in all cases. The powder starting material and mineralizer solutions were placed within silver ampoules, 2.5 in. in length with an O.D. of 1/4 in. and welded shut at both ends. These ampoules were then loaded into a Tuttle cold seal autoclave, with the remaining volume filled with water to serve as the counterpressure. Reactions were heated at 650 °C and 200 MPa for 7 days. After cooling the autoclave to room temperature, the resulting crystals were washed with deionized water and allowed to air dry. These reactions produced the desired compounds as phase pure products as characterized by single crystal and powder X-ray diffraction in all cases.

2.2. Structure determination

A summary of the crystallographic data for $KaAlGeO_4$, $KGaSiO_4$, and $KaGaGeO_4$ is provided in Table 1. Table 2 contains the summary of the crystallographic data for $RbAlSiO_4$, $CsAlGeO_4$, and $CsGaSiO_4$. The crystallographic data for $RbAlGeO_4$, $RbGaSiO_4$, $RbGaGeO_4$, and $CsAlSiO_4$ are included in the supporting information. Selected bond

Table 1
Crystallographic data for $KAlGeO_4$, $KGaSiO_4$, $KGaGeO_4$.

Empirical Formula	$KAlGeO_4$	$KGaSiO_4$	$KGaGeO_4$
Formula weight	202.67	200.91	245.41
Space group	$P6_3$	$P6_3$	$P6_3$
a, Å	18.424 (3)	18.1966 (6)	18.5273 (7)
c, Å	8.626 (2)	8.5322 (3)	8.6605 (4)
Volume, $Å^3$	2535.8 (11)	2446.65 (12)	2574.5 (2)
Z	24	24	24
Density (calculated), Mg/m^3	3.185	3.273	3.799
Parameters	255	255	254
θ range, deg	2.55 – 25.98	2.58 – 26.50	2.20 – 25.50
Reflections			
Collected	23558	39858	116569
Independent	3321	3385	3213
Observed, $I \geq 2\sigma(I)$	3237	3233	3014
R, int	0.0744	0.0392	0.0803
Final R, obs. Data			
R1	0.0338	0.0225	0.0404
wR2	0.0886	0.0568	0.1163
Final R, all Data			
R1	0.0349	0.0244	0.0469
wR2	0.0898	0.0575	0.1180
Goodness of fit of F^2	1.119	1.171	1.193
Flack Parameter	0.084 (17)	0.053 (13)	0.17 (5)

Table 2
Crystallographic data for $RbAlSiO_4$, $CsAlGeO_4$, and $CsGaSiO_4$.

Empirical Formula	$RbAlSiO_4$	$CsAlGeO_4$	$CsGaSiO_4$
Formula weight	204.54	296.48	294.72
Space group	$Pna2_1$	$Pna2_1$	$Pna2_1$
a, Å	8.7353 (4)	9.2846 (19)	9.2671 (19)
b, Å	9.2156 (4)	9.4757 (19)	9.3329 (19)
c, Å	5.3326 (2)	5.4861 (11)	5.4319 (11)
Volume, $Å^3$	429.28 (3)	482.66 (17)	469.80 (17)
Z	4	4	4
Density (calculated), Mg/m^3	3.165	4.080	4.167
Parameters	66	65	66
θ range, deg	3.21 – 26.48	3.07 – 26.00	3.10 – 25.47
Reflections			
Collected	12449	3933	3819
Independent	874	898	828
Observed, $I \geq 2\sigma(I)$	706	823	770
R, int	0.0324	0.0807	0.0531
Final R, obs. Data			
R1	0.0165	0.0353	0.0394
wR2	0.0443	0.0881	0.0882
Final R, all Data			
R1	0.0207	0.0420	0.0456
wR2	0.0468	0.0925	0.0909
Goodness of fit of F^2	1.151	1.086	1.254
Flack Parameter	0.254 (9)	0.11(7)	0.22 (13)

lengths and angles are provided in the supplemental information. In this work two different single crystal diffractometers were used. The first of these was a Rigaku AFC8 diffractometer equipped with a Mercury CCD and a Mo Kα (λ = 0.71073 Å) X-ray source. Collection and integration were managed using the Crystal Clear software program. [19] The second diffractometer used was a Bruker D8 Venture equipped with an Incoatec Mo Kα (λ = 0.71073 Å) microfocus source and Photon 100 CMOS detector. All data was collected at room temperature using phi and omega scans of 0.5° width. Data collection and integration were performed using Apex3. [20] The structures were solved by direct methods and refined by full-matrix least-squares on F^2 using the SHELXTL software suite.21 All atoms were refined anisotropically. In instances where atomic scattering factors could not reliably be used to distinguish the trivalent or tetravalent ions (for example, neighboring ions such as Al^{3+}/Si^{4+} or Ga^{3+}/Ge^{4+}), their identities were readily apparent based on the bond lengths to oxygen, and any potential order-disorder relationships were easily distinguished. Figures of the crystal structures were drawn using VESTA. [22] Data were deposited in CIF format to the joint CCDC/FIZ Karlsruhe deposition service, deposition numbers 2123881–2123892. Additional tabulated data of bond lengths and angles, atomic coordinates, and bond valence sum calculations are provided in the supporting information, Tables S.1-S.41. Verification of the structures and phase purity was made by powder X-ray diffraction (PXRD) performed using a Rigaku Ultima IV diffractometer with CuKα radiation (λ = 1.5406 Å) at 0.02° intervals at a rate of 1°/min from 5° to 65°.

2.3. Additional characterization

Second harmonic generation (SHG) data was obtained using a modified Kurtz experiment [23]. Crystals obtained in this work were sieved and sorted according to particle size (20, 38, 53, 75, 90, 106, 125, 180, and 250 μm). The size-separated samples were then placed in in-house fashioned sample holders. Measurements were taken using a 200 fs pulsed laser (Mira 900, Coherent) at 864 nm, with a peak power of 50 kW. A long wavelength pass filter (10LWF-650-B, Newport) was used to prevent any residual light from the pump laser at 532 nm (Verdi V6) while still allowing the generated pulse to pass on to the sample. After passing through a focusing lens, the beam was reflected off the size-separated samples in the in-house fashioned sample holder with a depth of 0.50 ± 0.05 mm. The reflected light was then collected by a large lens and passed through a short wavelength pass filter (10LWF-650-B, Newport) with a cutoff of 650 nm. A spectrometer (USB4000-VIS-NIR, Ocean Optics) was used across a range of 350 – 1000 nm, and the SHG peak was observed at 432 nm. The relative peak intensity was compared to the known SHG crystal KDP which had been measured in the same manner as the title compounds. A diagram of this experimental setup and sample holder is detailed in our prior work with wurtzite related structures [24].

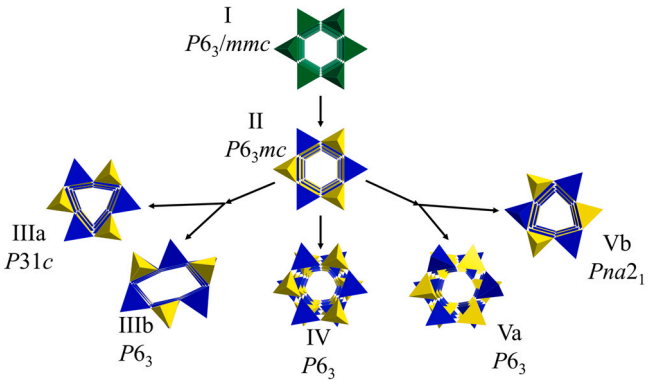

Fig. 1. Examples of degrees of freedom allowed within the tridymite framework.

3. Results and discussion

The large class of tridymite and stuffed tridymite structures can be broken down into several general categories based on types of degrees of freedom affecting the symmetry, namely ordering, channel shape, staggered or eclipsed tetrahedra, and finally, up-down relationships of the tetrahedra (Fig. 1). The parent archetype is the SiO_2 phase with eclipsed six membered rings of tetrahedra in an alternating UDUDUD pattern of the tetrahedra. This results in the centrosymmetric $P6_3/mmc$ space group (I). If half of the SiO_4 tetrahedra are replaced with ordered trivalent metal ions such as Al^{3+}, then the symmetry is lowered to the acentric $P6_3mc$ group (II). If the presence of the stuffing ion distorts the channels formed by the six membered rings to form either trigonal or kinked ring shapes, then the structure will adopt $P31c$ (IIIa) or chiral $P6_3$ symmetry (IIIb). If the channels retain their symmetry but the tetrahedra of subsequent layers along the *c*-axis are staggered instead of eclipsed then the symmetry can also be $P6_3$ (IV). The final degree of freedom is the up-down relationship of the tetrahedra within each six membered ring. At the highest symmetry the tetrahedra arrange in an UDUDUD array and can vary from UUUDDD to UUDDUD in $P6_3$ (Va) to $Pna2_1$ (Vb) respectively. All these degrees of freedom can be mixed and matched in various combinations to give a large array of structural possibilities as discussed herein. With the substitution of various sized tetrahedral structural components and alkali countercharge stuffing ions acting as experimental dials, the structures of the stuffed tridymite derivatives provide an excellent avenue for the exploration of the relationship of structure and SHG capabilities, given their tendency to form in acentric settings.

In all the cases discussed here, the hydrothermal synthesis approach is useful for both the synthesis and single crystal growth of the materials. The reaction temperature (650 °C), although high for aqueous processes, is relatively low compared to traditional solid state or flux growth reactions. The technique has the added advantage of being able to generate high quality single crystals that are often site-ordered. This attribute typically enables unambiguous structure determination which is critical for the understanding of these unusually subtle materials. The relatively large single crystals (Fig. 2) also ensure purity when evaluating other physical

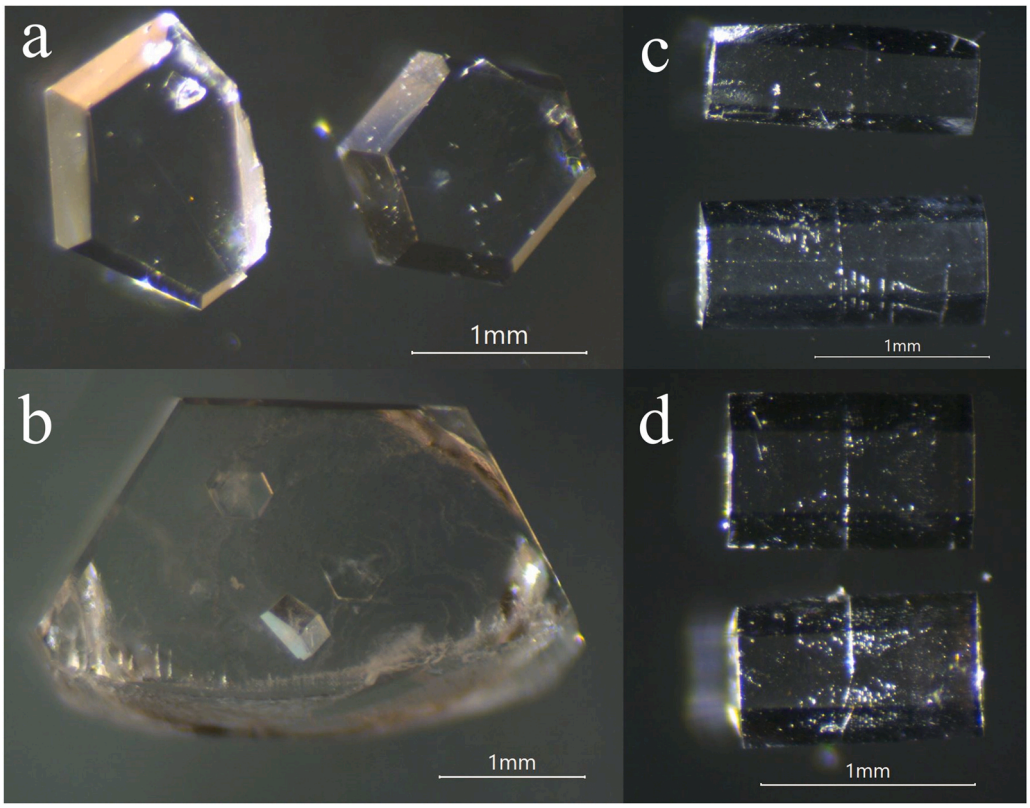

Fig. 2. Hydrothermally-grown single crystals of representative stuffed tridymite materials $KAlSiO_4$ (a), $KAlGeO_4$ (b), $KGaSiO_4$ (c), $KGaGeO_4$ (d).

parameters such an NLO coefficients, and of course if they are to be used in NLO applications, single crystals are essential.

3.1. The crystal structures of $KAlGeO_4$, $KGaSiO_4$, and $KGaGeO_4$

In the presence of potassium ions as mineralizer and stuffing ions, $KAlGeO_4$, $KGaSiO_4$, and $KGaGeO_4$ were prepared as phase pure crystals. All three were analyzed by single-crystal diffraction and were shown to crystallize in the noncentrosymmetric setting of $P6_3$ in a complex structure (Table 1). It should be noted that in our previous work with hydrothermal aluminosilicates, we found that the $KAlSiO_4$ formed in the $P31c$ structure type (type IIIa above). For $KAlSiO_4$ grown by flux methods, it was determined that it formed in a $P6_3$ space group, but one which is considerably different than those discussed here.

The structures of $KAlGeO_4$, $KGaSiO_4$, and $KGaGeO_4$ were found to be isostructural with one another in the chiral $P6_3$ space group (Fig. 3). While the space group of these structure is $P6_3$, which is the same space group setting as flux-grown $KAlSiO_4$, [25,26] the unit cell parameters are much larger and the structure much more complex. In the case of $KAlSiO_4$ a repeat unit of 5.15 Å is seen on the *a*-axis, [25] however when germanium or gallium substitutions are made this distance expands to over 18 Å. Although $KAlGeO_4$ has been previously reported in this setting however, to date no crystal structure is available for $KGaSiO_4$ and $KGaGeO_4$ [27,28]. This structure type is also reported multiple times for other tridymite derivatives [27–33]. The expanded unit cell is necessitated by the orientations of the tetrahedra within each cell. In the parent tridymite structure the tetrahedra in the six membered rings parallel to the *c*-axis maintain an UDUDUD geometry. In the unit cells of $KAlGeO_4$, $KGaSiO_4$, and $KGaGeO_4$ however, two types of six membered rings are present, with UDUDUD and UUUDDD rings, expressing variations of the "isomer" modification Vb in Fig. 1. There are two UDUDUD rings within the cell of the structure, surrounding

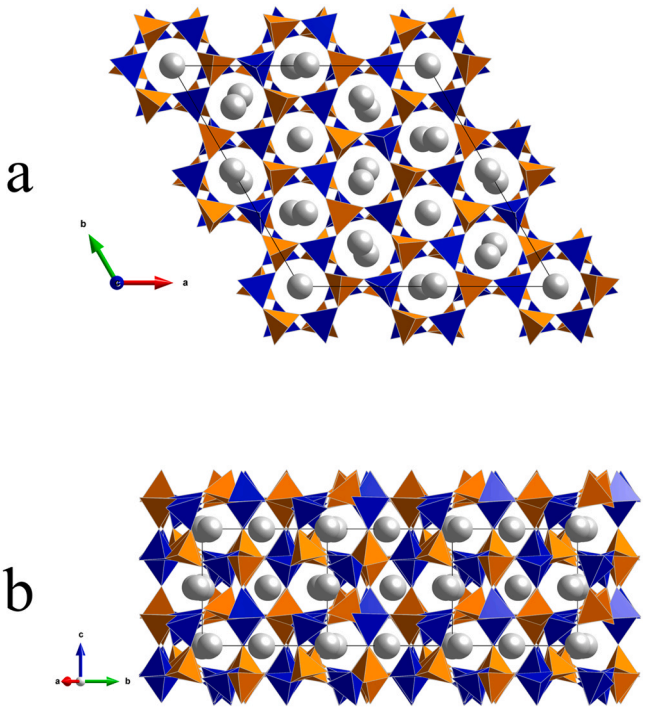

Fig. 3. Crystal structure of $KAlGeO_4$. a) Parallel to *c*-axis b) Parallel to *ab*-plane. Orange tetrahedra represent GeO_4 groups and blue represents the AlO_4 groups. Light gray spheres represent potassium atoms.

the three-fold rotation axis and at each of the corners, about the 6_3-screw axis. The UUUDDDD rings form around the 2_1-screw axis and in the regions between the three-fold axis and 6_3-screw axis. These rings form layers parallel to the *ab*-plane and are connected to their

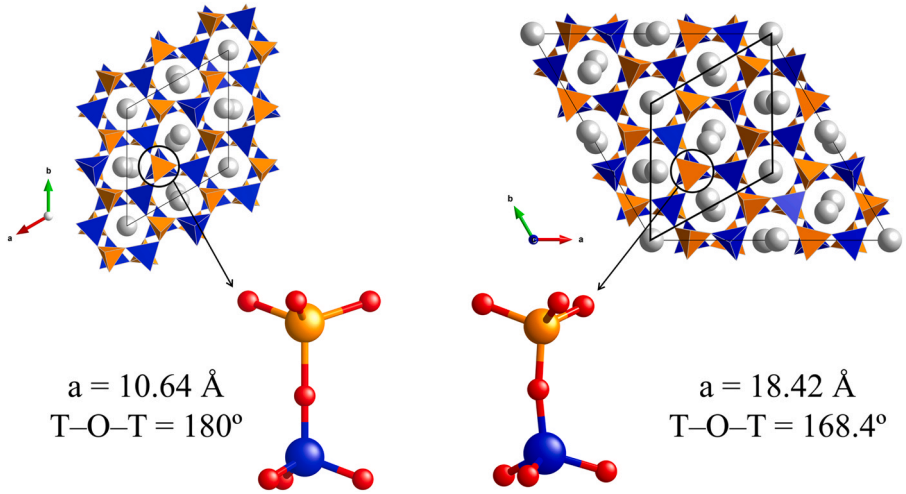

Fig. 4. Cell expansion required to move apical oxygen off rotational axis, as observed in $KAlGeO_4$, $KGaSiO_4$, and $KGaGeO_4$ (right) versus an alternative arrangement of $KAlGeO_4$ adopting the $RbMnVO_4$ structure type (left).

neighboring layers through the apical oxygen atoms. The repeating layers are staggered relative to each other, rather than the eclipsed orientation assumed by trigonal $KAlSiO_4$. The connections to the subsequent layers formed by the UUUDDD six-membered rings form ten-membered rings just off the *a*-axis (Fig. 3b).

These structural combinations generate a large cell to accommodate all of the variations of the different ring conformations. For comparison $RbMnVO_4$ has also been solved in a related $P6_3$ structure but with a ≈ 11.26 Å and the general structure is somewhat similar to that of the larger cells described here [15]. In the relatively smaller 11 Å cell however, the apical oxygen at the 2b site tends to have very broad anisotropic displacement parameters or be split over three sites. By splitting off the ideal three-fold rotation axis, the T – O – T bond will not have to adopt a less desirable 180° angle. If the cell is then tripled by the expansion of the *a*-axis by √3 then the split oxygen sites can be moved away from the three-fold rotation axis which allows them to still be ordered within the structure (Fig. 4) [27,28,34].

Bond lengths and angles for $KAlGeO_4$, $KGaSiO_4$, and $KGaGeO_4$ are provided in Tables S.1 – S.6. and range from 1.63 Å to 1.82 Å for the unique tetrahedral sites, depending on the metal ion present, and all are typical for these types of tetrahedra. The O – T – O angles of the AlO_4, GaO_4, SiO_4, and GeO_4 tetrahedra show only minor deviations from the ideal angles of 109.5°, regardless of the overall geometry in the unit cell. Each structure has six unique potassium sites, with three at general positions resulting in irregular polyhedra, and three at special positions coordinated to three sets of symmetry related oxygen atoms, forming a tri-capped octahedron.

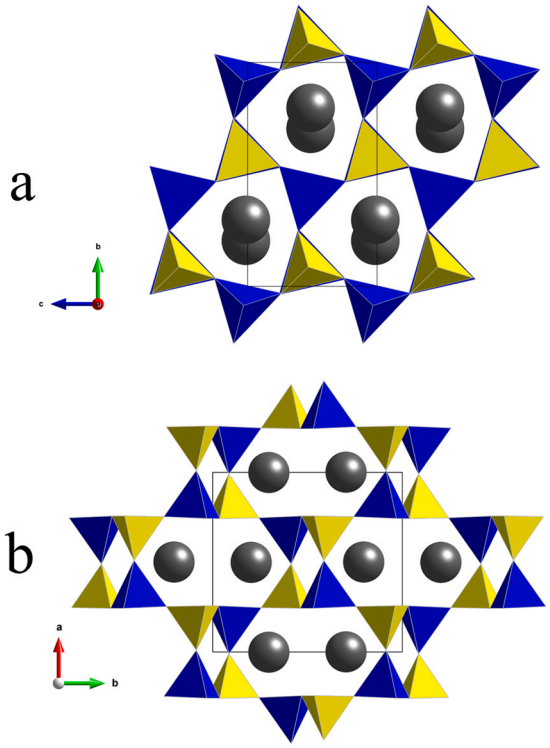

Fig. 5. Crystal structures of $RbAlSiO_4$. a) Parallel to *c*-axis. b) Parallel to *ab*-plane. Yellow tetrahedra represent SiO_4 groups and blue represents the AlO_4 groups. Dark gray spheres represent rubidium atoms.

3.2. The crystal structures of $RbAlSiO_4$, $CsAlGeO_4$, and $CsGaSiO_4$

The structure of $RbAlSiO_4$ is one of some ambiguity which was initially investigated by Klaska and Jarchow in 1975 [35], and was reinvestigated more recently, confirming the original structure in the acentric $Pna2_1$ space group [36]. If the substitution of aluminum or silicon by larger tetrahedral ions is accompanied by the substitution of cesium in place of rubidium, as in $CsAlGeO_4$ and $CsGaSiO_4$, the polar acentric $Pna2_1$ space group is also maintained. This structure breaks the symmetry of ideal tridymite in three of the four possible degrees of freedom (Fig. 5). The first is by the ordering of the tetrahedral $3^+/4^+$ sites (Fig. 1. II). The second is by the bending of the hexagonal rings into ditrigonal rings as is seen in many stuffed tridymite variants (Fig. 1. IIIa). Finally, and most drastically, the orientation of the tetrahedra that compose the rings has been altered to accommodate the larger stuffing cation size of rubidium (Fig. 1. Vb). In the parent tridymite structure, the tetrahedra that compose the hexagonal rings are arranged in the standard fashion of UDUDUD. The ditrigonal rings within the framework of $RbAlSiO_4$, $CsAlGeO_4$, and $CsGaSiO_4$ however, are oriented in an UUUDDD manner with respect to the *bc*-plane. While the standard arrangement of the tetrahedra in tridymite creates additional six membered rings along the *a* and *b* axis, the UUUDDD ordering creates eight-membered rings parallel to the *ab* plane (Fig. 5b). With neighboring tetrahedra of like orientation connected to their mirror equivalents through the apical oxygen site, four membered rings are formed. These four membered rings can also be seen in Fig. 5b to make up the sides of the eight-membered rings.

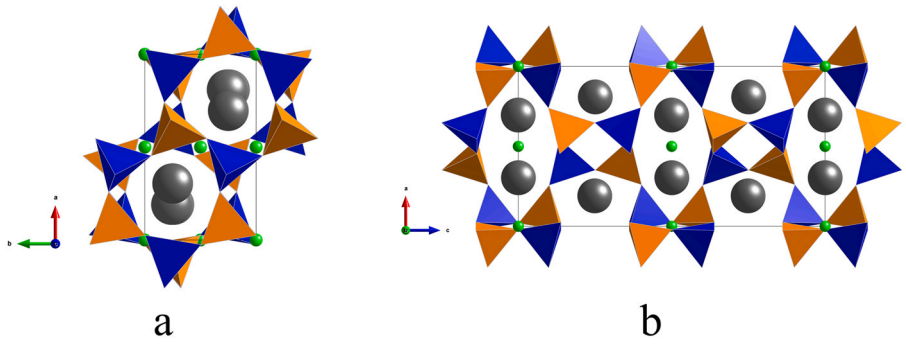

Fig. 6. Structure of $RbAlGeO_4$, ($P2_1/c$). a) Parallel to the *c*-axis b) Parallel to the *ab*-plane. Orange tetrahedra represent GeO_4 groups, blue represents the AlO_4 groups. Dark gray spheres represent rubidium and green spheres represent inversion centers.

Table 3
SHG and structural modifications in stuffed tridymites of the present study.

Formula	Space Group	Structural deviations from parent stuffed Tridymite	SHG relative to KDP
$KAlSiO_4$[16]	$P31c$	Ordered Tetrahedra (II), Ditrigonal rings (IIIa)	22%
$KAlGeO_4$	$P6_3$	Ordered Tetrahedra (II), Ditrigonal rings (IIIa), Staggered (IV), Both UDUDUD (Va) and UUUDDD (Vb)	4%
$KGaSiO_4$	$P6_3$	Ordered Tetrahedra (II), Ditrigonal rings (IIIa), Staggered (IV), Both UDUDUD (Va) and UUUDDD (Vb)	5%
$KGaGeO_4$	$P6_3$	Ordered Tetrahedra (II), Ditrigonal rings (IIIa), Staggered (IV), Both UDUDUD (Va) and UUUDDD (Vb)	4%
$RbAlSiO_4$	$Pna2_1$	Ordered Tetrahedra (II), Ditrigonal rings (IIIa), UUUDDD (Vb)	38%
$CsAlGeO_4$	$Pna2_1$	Ordered Tetrahedra (II), Ditrigonal rings (IIIa), UUUDDD (Vb)	21%
$CsGaSiO_4$	$Pna2_1$	Ordered Tetrahedra (II), Ditrigonal rings (IIIa), UUUDDD (Vb)	25%

The previous published structures of $RbAlSiO_4$ both contained twinning by reticular merohedry with the reflection twin planes (110) and (310) which accounted for the earlier difficulty in obtaining an unambiguous structural solution [35,36]. In our crystals however, the PLATON software package was used to search for twins, but none were found, either for $RbAlSiO_4$ or the isostructural $CsAlGeO_4$, and $CsGaSiO_4$ [37]. While the Flack parameter of $RbAlSiO_4$ is somewhat high (0.3), the crystals clearly demonstrated second harmonic generation (see below), confirming the noncentrosymmetric structure.

The bonding environments for $RbAlSiO_4$, $CsAlGeO_4$, and $CsGaSiO_4$ are provided in Tables S.7 – S.9. The tetrahedral sites in each structure are well ordered, with the expected M^{3+}-O and M^{4+}-O bond distances. In $RbAlSiO_4$ the average rubidium to oxygen distance is 3.29 Å within the channels formed down the *a*- and *c*-axes, while in $CsAlGeO_4$ and $CsGaSiO_4$ the average cesium to oxygen distance is 3.40 Å for both structures, enabling the relatively large monovalent ions to fit in the channels without inducing further distortion.

While the stuffed tridymite system may be attractive for systematically varying the structure/NLO property relationship of related materials, it unfortunately does not always yield acentric materials. This is particularly true as the metal ions get larger. While $RbAlSiO_4$ forms in the non-centrosymmetric setting of $Pna2_1$, increasing the size of the tetrahedral units by substitution of germanium and gallium into the silicon and aluminum sites respectively ($RbAlGeO_4$ and $RbGaSiO_4$) causes the structure to distort to maintain the environment about the rubidium cations. This modification is facilitated by one of the structural degrees of freedom present in this structural family, the staggering of the tetrahedra along the principal axis (Fig. 6). In $RbAlGeO_4$, $RbGaSiO_4$, and $RbGaGeO_4$ this staggered conformation features pairs of eclipsed tetrahedra that stagger along the *a*-axis. This leads to the centrosymmetric setting of $P2_1/c$, by the introduction of inversion centers between these pairs. This setting is also observed in the structure of $LiNH_4SO_4$ [38].

The nominally "simplest" stuffed tridymite $NaAlSiO_4$ formula has a long and convoluted structural history which is highly sensitive to the growth method (if manmade) or mineral origin, and most of those are also acentric [17]. In our hands however, Na^+ is the only ion that shows a reduced tendency to adopt acentric structures among the tridymites, in part because of the tendency for the *B*/*C* ions to disorder. For example, hydrothermally grown $NaAlSiO_4$ forms in the centrosymmetric $P2_1/n$ lattice only because the Al^{3+} and Si^{4+} ions fully disorder. If the two ions ordered, the structure would have an acentric $P2_1$ lattice. It is important to note that the addition of even a small amount of K^+ ion to the Na^+ tridymite formula leads to a whole new range of structures, most of which are again acentric [17]. This further begs the question of whether other combinations of mixed stuffing ions will lead to new acentric tridymite derivatives. Crystallographic data for the centrosymmetric compounds is reported in the Supplemental Information, Table S.10.

3.3. Optical properties

The structural degrees of freedom inherent to the stuffed tridymite family when combined with their tendency to adopt acentric settings allows for study in the relationship of structure to SHG ability (Table 3). We were aware going into this study that it was unlikely that we would observe large NLO coefficients because of the low polarizability of the anionic groups. Our goal instead was to assess the overall NLO behavior and to probe the structural possibilities within this structurally complex class of compounds. The acentric crystals of this study were analyzed using a modified Kurtz experiment and compared with the known SHG material KH_2PO_4 (KDP) at particle sizes up to 250 µm. The centrosymmetric crystals detailed earlier were also analyzed to ensure that the symmetry of the systems was not over-assumed. From this study phase matching ability and SHG ability relative to KDP were able to be ascertained. In addition to the previously discussed structures, hydrothermally-synthesized $KAlSiO_4$ was also analyzed [17]. The hydrothermally-synthesized sodium tridymite analogues $NaAlSiO_4$ [17], $NaAlGeO_4$ [28], and $NaGaSiO_4$ are all centrosymmetric in the setting of $P2_1/n$ and showed no NLO conversion as would be expected.

The resultant graph of the modified Kurtz experiment of a typical example of hydrothermally synthesized $KAlSiO_4$ is presented in Fig. 7a. This plot is characteristic of a phase matching material. By comparing the SHG ability of a standard having the same particle size with a relative efficiency comparison may be made. Using this method $KAlSiO_4$ can be shown to have an efficiency of converting

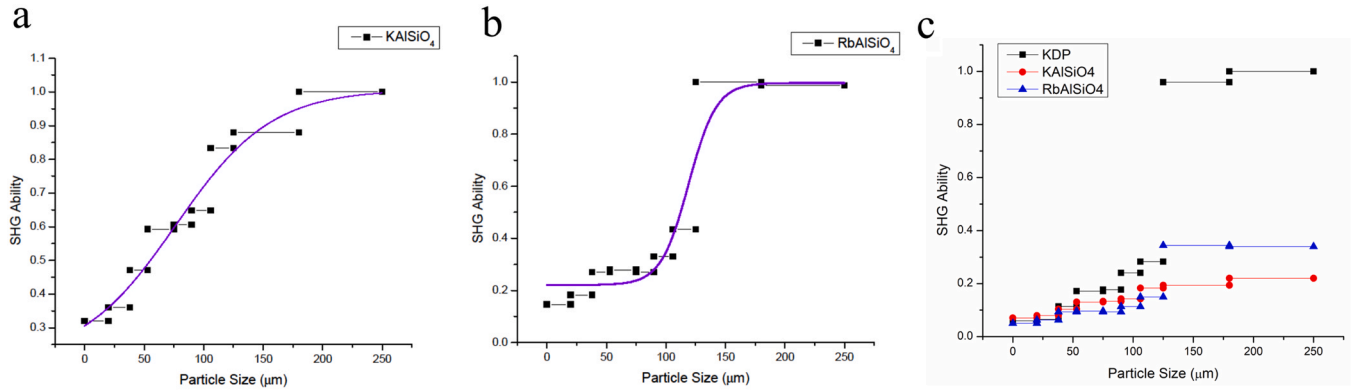

Fig. 7. Powder SHG measurements of $KAlSiO_4$ (a) and $RbAlSiO_4$ (b).

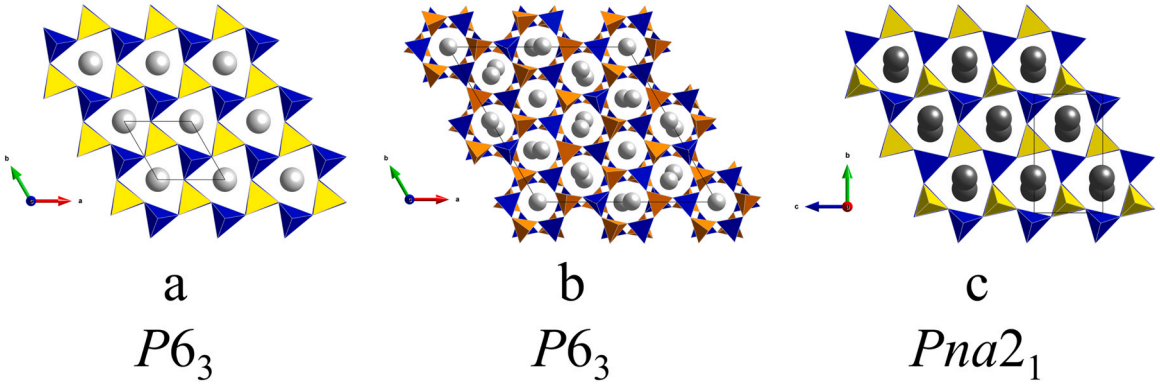

Fig. 8. Comparative views of the crystal structures of a) $KAlSiO_4$; b) $KAlGeO_4$; and c) $RbAlSiO_4$ down the *c*-axis. Yellow tetrahedra represent SiO_4 groups, GeO_4 are represented by orange tetrahedra, and blue represents the AlO_4 groups. Light gray spheres represent potassium atoms and dark gray spheres represent rubidium atoms.

864–432 nm at 22% relative the power of the common NLO material KDP (Fig. 7c). This experiment was then conducted on the other potassium species: $KAlGeO_4$, $KGaSiO_4$, and $KGaGeO_4$. These materials were found to produce a relatively low degree of NLO conversion. As these three crystals are isostructural it is no surprise that they behave similarly in terms of NLO capabilities. While the structures of $KAlGeO_4$, $KGaSiO_4$, and $KGaGeO_4$ were discussed earlier, an examination of $KAlSiO_4$ is useful to explore the relationship of structure to SHG. If we look at these structural differences in terms of the degrees of freedom as illustrated in Fig. 1 there are two notable differences. In looking down the *c*-axis of both structures (Fig. 8a, b) it is immediately apparent that $KAlSiO_4$ features an eclipsed tetrahedral arrangement while $KAlGeO_4$, $KGaSiO_4$, and $KGaGeO_4$ are staggered. The second degree of freedom in which these structures differ is the conformational difference of UDUDUD in $KAlSiO_4$ and the more complicated structures of $KAlGeO_4$, $KGaSiO_4$, and $KGaGeO_4$ which contain rings of UDUDUD and UUUDDD. In viewing these structures down the *a*-axis (perpendicular to the layers of hexagonal rings) (Fig. 9a, b) a tilting of the tetrahedra can be seen in $KAlGeO_4$, $KGaSiO_4$, and $KGaGeO_4$. We postulate that this structural complexity is responsible for the relatively low NLO efficiency because the anionic groups responsible for the NLO conversion do not overlap each other as well as in the simpler structure. In this case the anionic alignment cannot reinforce the NLO conversion process.

The third isostructural group to be investigated by this study was that of $RbAlSiO_4$, $CsAlGeO_4$, and $CsGaSiO_4$. Once more using the

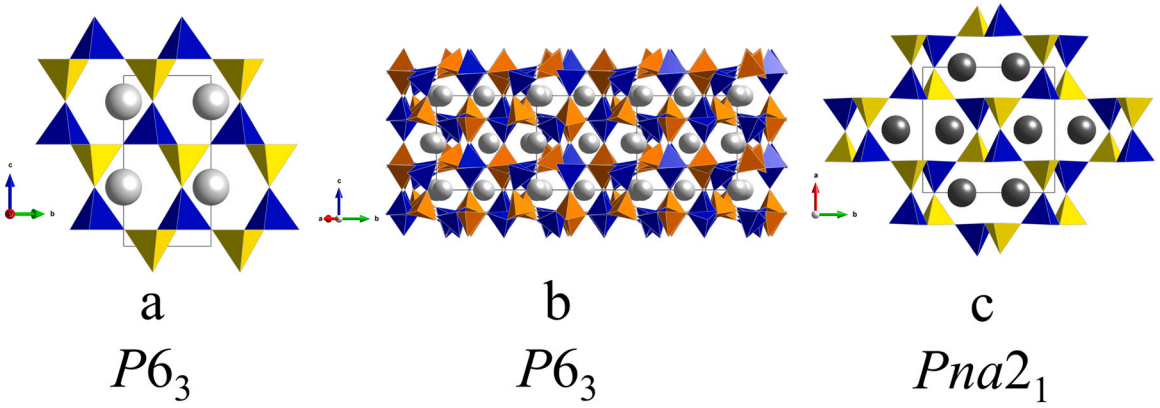

Fig. 9. Comparative views of the crystal structures of a) $KAlSiO_4$; b) $KAlGeO_4$; and c) $RbAlSiO_4$ parallel to the *ab*-plane. Yellow tetrahedra represent SiO_4 groups, GeO_4 are represented by orange tetrahedra, and blue represents the AlO_4 groups. Light gray spheres represent potassium atoms and dark gray spheres represent rubidium atoms.

Kurtz experiment, $RbAlSiO_4$ was found to be phase matching as can be seen in Fig. 7b. In this case $RbAlSiO_4$ was found to have a power relative to 38% of KDP at doubling from 864 nm to 432 nm (Fig. 7c). Comparisons of $CsAlGeO_4$, and $CsGaSiO_4$ with KDP were also made with relative efficiencies of 21% and 25% respectively. When looking at differences between the structures of $KAlSiO_4$ (Fig. 8a) and $RbAlSiO_4$ (Fig. 8c) in terms of separation via the aforementioned degrees of freedom there is only one notable distinction, which is in the form of the conformational isomers UDUDUD in $KAlSiO_4$ and UUUDDD in $RbAlSiO_4$. While this discrepancy also was observed with $KAlGeO_4$ this comparison is more direct due to the relative simplicity of the $RbAlSiO_4$ structure. It is this simplicity that may be the source of the slightly larger SHG conversion, even though $RbAlSiO_4$ is in a lower symmetry, $Pna2_1$ versus $P31c$. It must be borne in mind however, that this NLO data are all based on initial results using a powdered material (< 250 μm). In order to establish a better comparison of these materials, large single crystals would need to be grown to access their SHG coefficient more accurately. These initial relative efficiencies are within the same order of magnitude and may indicate only a small relationship between structural arrangement and SHG ability with similar structural units.

4. Summary and conclusions

This paper reports a systematic investigation of a class of stuffed tridymites $ABCO_4$ where *A* is a range of alkali ions and *B* and *C* are group 13 and 14 elements respectively. The structures are based on the parent tridymite, whose idealized structure forms in the high symmetry $P6_3/mmc$ space group. It consists of eclipsed tetrahedra forming columns of six membered rings. These columns are parallel to the c-axis and are where the "stuffing" ions are located. There are many variations of the structure, most of which can be explained by symmetry lowering of the parent compound by ordering of the *B* and *C* ions, staggering the tetrahedra, varying the shape of the six membered rings, and/or varying the relative orientation of the tetrahedral building blocks relative to the *ab*-plane. All these symmetry breaking steps can be mixed and matched to form a large array of structure types. The stuffed tridymites are particularly attractive for NLO applications because these structural variations lead to an inordinately high number of acentric space groups, making it a promising class for systematic structure property relationships.

In most cases the products can be synthesized using a high temperature (650°C) hydrothermal method, and form as high-quality single crystals in good yields. The materials are usually well ordered on the *B* and *C* sites and often form in polar acentric space groups. This is typical of the large class of tridymite derivatives, and it opens the door for not only new classes of NLO compounds, but many of these compounds can also act jumping off points for new ferroelectrics, multiferroics, spintronics and many other nonclassical materials. This makes the systematic investigation of the structural relationships worthwhile and important. Despite the limited palate of building blocks in tridymites (exclusively tetrahedra), there is an enormous range of structural possibilities within the stuffed tridymite class.

Apropos to this work, the actual structures we obtain are often acentric. This seems to be particularly true for crystals containing the smaller lighter elements. As the metal ions get larger there appears to be a somewhat increased tendency to form either centrosymmetric structures or *B*/*C* disordered structures which decreases the tendency to form acentric lattices. With this in mind we decided to examine the structural possibilities systematically across the range of possible elements in $ABCO_4$. We found that most of the structures are acentric and most can be explained using the symmetry breaking guidelines described herein.

Across the matrix of $ABCO_4$ elemental possibilities, the range structures adopted is very large. All the structures can be derived from the parent $P6_3/mmc$ structure type. The alkali ions become located in the six-membered channels down the *c* axis, while half of the silicon atoms *C* assume the trivalent atomic identity *B*. If the *B* and *C* sites order then there are a range of ring distortions, stacking patterns and up/down relationships that can add to the structural possibilities, and nearly all of those are acentric. These symmetry breaking operations can be mixed and matched to account for most of the tridymite derivatives we observe. We surveyed most of the elemental combinations of the alkali ions with Group 13 and 14 ions, but we have not yet examined many mixed alkali ion materials. Given the success of our earlier work on Na^+/K^+ mixed species, this work is certainly warranted. It appears that one of the most important factors in these compounds is the ordering of the *B* and *C* sites. If they disorder then most of the symmetry breaking processes are nullified and centrosymmetric space groups are observed. Using the hydrothermal approach, we can grow relatively large, high quality single crystals in most cases, allowing for subsequent development of any promising materials.

We used the Kurtz method to obtain preliminary NLO efficiencies of the acentric tridymites. In all cases the NLO conversions are relatively small. This is not unexpected this since the anionic building blocks responsible for the conversions are not very polarizable. They do confirm that the acentric space groups are correctly assigned and provide some rough guidelines for subsequent NLO crystal design. In addition to NLO conversion there is a large array of other interesting and important materials including multiferroics, frustrated magnets, skyrmions and many others that depend in some way on acentric and polar structure types. As such a deeper systematic understanding of the structural factors of acentric materials will continue to be important.

CRediT authorship contribution statement

Rylan J. Terry: Investigation, Methodology, Writing – original draft. **Daniel Vinton:** Investigation. **Colin D. McMillen:** Methodology, Writing – review & editing. **Xiangfeng Chen:** investigation. **Lin Zhu:** Supervision. **Joseph W. Kolis:** Supervision, Funding acquisition, Writing – review & editing.

Declaration of Competing Interest

The authors declare that they have no known competing financial interests or personal relationships that could have appeared to influence the work reported in this paper.

Acknowledgements

We acknowledge the support of the NSF DMR DMR-1808371. Any opinions, findings and conclusions or recommendations expressed in this material are those of the author(s) and do not necessarily reflect those of the National Science Foundation."

Appendix A. Supporting information

Supplementary data associated with this article can be found in the online version at doi:10.1016/j.jallcom.2022.164634.

References

[1] P.S. Halasyamani, K.R. Poeppelmeier, Noncentrosymmetric oxides, Chem. Mater. 10 (10) (1998) 2753–2769, https://doi.org/10.1021/cm980140w
[2] K.M. Ok, E.O. Chi, P.S. Halasyamani, Bulk characterization methods for noncentrosymmetric materials: second-harmonic generation, piezoelectricity, pyroelectricity, and ferroelectricity, Chem. Soc. Rev. 35 (8) (2006) 710–717, https://doi.org/10.1039/B511119F
[3] W. Zhang, H. Yu, H. Wu, P.S. Halasyamani, Phase-matching in nonlinear optical compounds: a materials perspective, Chem. Mater. 29 (7) (2017) 2655–2668, https://doi.org/10.1021/acs.chemmater.7b00243

[4] A.K.A. Pryde, M.T. Dove, On the sequence of phase transitions in tridymite, Phys. Chem. Min. 26 (2) (1998) 171–179, https://doi.org/10.1007/s002690050174
[5] D.C. Palmer, Stuffed derivatives of the silica polymorphs, Rev. Mineral. Geochem. 29 (1) (1994) 83–122.
[6] R.N. Abbot, K.Al.SiO.4 stuffed derivatives of tridymite; phase relationships, Am. Min. 69 (5–6) (1984) 449–457.
[7] G. Wallez, F. Lucas, J.-P. Souron, M. Quarton, Potassium-zinc monophosphate: an original polymorphic tridymite derivate, Mater. Res. Bull. 34 (8) (1999) 1251–1261, https://doi.org/10.1016/S0025-5408(99)00124-5
[8] R. Hammond, J. Barbier, Structural chemistry of NaCoPO4, Acta Cryst. B 52 (3) (1996) 440–449, https://doi.org/10.1107/S0108768195016259
[9] X. Bu, T.E. Gier, G.D. Stucky, A new polymorph of lithium zinc phosphate with the cristobalite-type framework topology, J. Solid State Chem. 138 (1) (1998) 126–130, https://doi.org/10.1006/jssc.1998.7762
[10] P. Feng, X. Bu, S.H. Tolbert, G.D. Stucky, Syntheses and characterizations of chiral tetrahedral cobalt phosphates with zeolite ABW and related frameworks, J. Am. Chem. Soc. 119 (10) (1997) 2497–2504, https://doi.org/10.1021/ja9634841
[11] G. Nénert, J. Bettis, R. Kremer, H. Ben Yahia, C. Ritter, E. Gaudin, O. Isnard, M.-H. Whangbo, Magnetic properties of the $RbMnPO_4$ zeolite-ABW-type material: a frustrated zigzag spin chain, Inorg. Chem. 52 (16) (2013) 9627–9635, https://doi.org/10.1021/ic401408f
[12] C.D. Johnson, D.E. Macphee, J. Feldmann, New low temperature synthetic route to an ammonium zinc arsenate zeolite analogue with an ABW-type structure, Inorg. Chem. 41 (14) (2002) 3588–3589, https://doi.org/10.1021/ic025603l
[13] M. Andratschke, K.-J. Range, C. Weigl, U. Schießl, F. Rau, Die kristallstruktur von $TlZnPO_4$ Und $TlZnAsO_4$ / the crystal structure of $TlZnPO_4$ and $TlZnAsO_4$, Z. Naturforsch. B 49 (9) (1994) 1282–1288, https://doi.org/10.1515/znb-1994-0920
[14] M. Andratschke, K.-J. Range, U. Klement, Die kristallstruktur von NaZnAsO4 / the crystal structure of $NaZnAsO_4$, Z. Naturforsch. B 48 (7) (1993) 965–968, https://doi.org/10.1515/znb-1993-0719
[15] H. Ben Yahia, E. Gaudin, J. Darriet, Synthesis, structures and magnetic properties of the new vanadates $AgMnVO_4$ and $RbMnVO_4$, J. Solid State Chem. 181 (11) (2008) 3103–3109, https://doi.org/10.1016/j.jssc.2008.08.001
[16] H.D. Flack, Chiral and achiral crystal structures, Helv. Chim. 86 (4) (2003) 905–921, https://doi.org/10.1002/hlca.200390109
[17] Terry, R.J.; McMillen, C.D.; Kolis, J.W. Hydrothermal Single Crystal Growth and Structural Investigation of the Nepheline and Kalsilite Stuffed Tridymite Species. J. Chem. Crystallogr. in press. doi: 10.1007/s10870-022-00940-6.
[18] P. Daniels, C.A. Fyfe, Al,Si order in the crystal structure of α-eucryptite ($LiAlSiO_4$), Am. Min. 86 (3) (2001) 279–283, https://doi.org/10.2138/am-2001-2-310
[19] Crystal Clear, Mercury CCD Automated Imaging System; Rigaku Corp.: Oren, UT, 2001.
[20] APEX3; Bruker AXS: Madison, WI, 2015.
[21] G.M. Sheldrick, Crystal structure refinement with SHELXL, Acta Cryst. C 71 (1) (2015) 3–8, https://doi.org/10.1107/S2053229614024218
[22] K. Momma, F. Izumi, VESTA 3 for three-dimensional visualization of crystal, volumetric and morphology data, J. Appl. Cryst., J. Appl. Crystallogr. 44 (6) (2011) 1272–1276, https://doi.org/10.1107/S0021889811038970
[23] S.K. Kurtz, T.T. Perry, A powder technique for the evaluation of nonlinear optical materials, J. Appl. Phys. 39 (8) (1968) 3798–3813, https://doi.org/10.1063/1.1656857
[24] R.J. Terry, C.D. McMillen, X. Chen, Y. Wen, L. Zhu, G. Chumanov, J.W. Kolis, Hydrothermal single crystal growth and second harmonic generation of Li_2SiO_3, Li_2GeO_3 and $Li_2Si_2O_5$, J. Cryst. Growth 493 (2018) 58–64, https://doi.org/10.1016/j.jcrysgro.2018.02.028
[25] Y. Andou, A. Kawahara, The refinement of the structure of synthetic kalsilite, Mineral. J. 12 (4) (1984) 153–161, https://doi.org/10.2465/minerj.12.153
[26] A.J. Perrotta, S.M. Smith, J.V. Smith, The crystal structure of kalsilite, $KAlSiO_4$, Mineral. Mag. 35 (272) (1965) 588–595, https://doi.org/10.1180/minmag.1965.035.272.02
[27] G. Lampert, R. Bohm, The crystal structure of $KAlGeO_4$, Z. Krist. 176 (1–2) (1986) 29–33, https://doi.org/10.1524/zkri.1986.176.1-2.29
[28] P.A. Sandomirskii, S.A. Meshalkin, I.V. Rozhdestvenskaya, L.N. Dem'yanets, T.G. Uvarova, Crystal structures of the D-Phase of K{$AlGeO_4$} and the C-Phase of Na{$AlGeO_4$}, Sov. Phys. Crystallogr. 31 (5) (1986) 522–527.
[29] I.A. Gudkova, Z.A. Solodovnikova, S.F. Solodovnikov, E.S. Zolotova, N.V. Kurat'eva, Phase formation in Li_2MoO_4-K_2MoO_4-$MMoO_4$ (M = Ca, Pb, Ba) systems and the crystal structure of α-$KLiMoO_4$, Russ. J. Inorg. Chem. 56 (9) (2011) 1443, https://doi.org/10.1134/S0036023611090075
[30] M. Andratschke, K.-J. Range, H. Haase, U. Klement, Die kristallstruktur von α-$KZnPO_4$ / the crystal structure of α-$KZnPO_4$, Z. Naturforsch. B 47 (9) (1992) 1249–1254, https://doi.org/10.1515/znb-1992-0906
[31] L. Perez, M. Luis, F. Kubel, H. Schmid, Crystal growth and X-ray structure of metastable a-$KCoPO_4$, Z. Nat. 49 (9) (1994) 1256–1262.
[32] R. Hammond, J. Barbier, Low-temperature $KFeGeO_4$, Acta Crystallogr. C 55 (7) (1999), https://doi.org/10.1107/S0108270199099254
[33] V. Kahlenberg, R.X. Fischer, J.B. Parise, The stuffed framework structure of $BaGa2O_4$, J. Solid State Chem. 154 (2) (2000) 612–618, https://doi.org/10.1006/jssc.2000.8903
[34] W. Sun, H. Li, B. Zheng, R. Pang, L. Jiang, S. Zhang, C. Li, Electronic structure and photoluminescence properties of a novel single-phased color tunable phosphor $KAlGeO_4$:Bi^{3+}, Eu^{3+} for WLEDs, J. Alloy. Compd. 774 (2019) 477–486, https://doi.org/10.1016/j.jallcom.2018.10.087
[35] R. Klaska, O. Jarchow, Die Kristallstruktur Und Die Verzwillingung von $RbAlSiO_4$, Z. Krist. Cryst. Mater. 142 (1–6) (1975) 225–238, https://doi.org/10.1524/zkri.1975.142.16.225
[36] G.D. Gatta, N. Rotiroti, P.F. Zanazzi, M. Rieder, M. Drabek, Z. Weiss, R. Klaska, Synthesis and crystal structure of the feldspathoid $CsAlSiO_4$: an open-framework silicate and potential nuclear waste disposal phase, Am. Miner. 93 (7) (2008) 988–995, https://doi.org/10.2138/am.2008.2729
[37] A.L. Spek, Single-crystal structure validation with the program PLATON, J. Appl. Cryst. 36 (1) (2003) 7–13, https://doi.org/10.1107/S0021889802022112
[38] H. Mashiyama, H. Kasano, Refined crystal structure of $LiNH_4SO_4$ including hydrogen atoms in phases II and III, J. Phys. Soc. Jpn. 62 (1) (1993) 155–162, https://doi.org/10.1143/JPSJ.62.155